International Journal of Secondary Metabolite
2024, Vol. 11, No. 4, 812–832
https://doi.org/10.21448/ijsm.1485796
journal homepage: https://dergipark.org.tr/en/pub/ijsm
Research Article

Comparison of high antioxidant ZnONPs produced from different fungi as alternative biomaterials

Olcay Gençyılmaz[1*], **Mohanad Fawzi Mutar Mutar**[1]

[1]Çankırı Karatekin University, Department of Physics, Çankırı, Türkiye

ARTICLE HISTORY

Received: May 17, 2024
Accepted: Aug. 22, 2024

KEYWORDS

ZnONPs,
Green synthesis,
Fungi,
Antimicrobial,
FESEM.

Abstract: In this study, zinc oxide nanoparticles (ZnONPs), a promising alternative biomaterial, were synthesized using a non-toxic, cost-effective green synthesis approach using various fungal species (*Penicillium citrinum, Fusarium solani, Aspergillus flavus* and *Aspergillus niger)*. The effect of different fungal species on the structural, optical, morphological and antimicrobial properties of ZnO nanoparticles (ZnONPs) was compared. ZnO nanoparticles (ZnONPs) crystallized in a hexagonal wurtzite structure with grain sizes ranging from 45 to 61 nm. Fungal species had a significant effect on the surface plasmon resonance (SPR) peak observed at 302 nm. ZnONPs were obtained in different morphologies such as nanodiscs, nanospheres, nanorchins and nanonuts, and it was determined that fungal species had a significant effect on these structures. The antibacterial activity of ZnONPs against *Candida albicans*, *Streptococcus mutans*, *Pseudomonas aeruginosa*, *Eosinophilic pneumonia* and *Staphylococcus aureus* was investigated. The effect of these nanoparticle shapes on antibacterial activity was evaluated. ZnONPs were found to have a significant antimicrobial effect especially on *Candida albicans* and *Streptococcus mutans*. ZnONPs produced only with *Aspergillus niger* fungus were found to have a strong antimicrobial effect especially on *Staphylococcus aureus*. Based on these results, the biosynthesis of ZnO nanoparticles (ZnONPs) using *Penicillium citrinum*, *Fusarium solani*, *Aspergillus flavus* and *Aspergillus niger* fungal species is proposed for the production of ZnONPs as a biomaterial with remarkable antibacterial properties and various morphologies.

1. INTRODUCTION

In recent years, numerous studies have been conducted on the production and characterization of nanomaterials to discover intriguing aspects of nanotechnology. In particular, the distinctive physical characteristics of metallic nanoparticles (MNPs) or metal oxide nanoparticles (MONPs) have garnered attention. In response to environmental concerns associated with traditional chemical methods for producing these nanoparticles, biogenic synthesis has emerged as a viable alternative. Green synthesis is a clean, non-toxic, and cost-effective method that utilizes plants and microorganisms to synthesize nanoparticles (NPs) (Abdelhakim *et al*., 2020).

Due to their good conductivity, chemical stability, catalytic properties, photonic and optical properties, ZnO is among the most extensively researched metal oxide nanoparticles (MONPs)

*CONTACT: Olcay GENÇYILMAZ ogencyilmaz@karatekin.edu.tr Çankırı Karatekin University, Department of Physics, Çankırı, Türkiye

© The Author(s) 2024. Open Access This article is licensed under a Creative Commons Attribution 4.0 International License. To view a copy of this licence, visit http://creativecommons.org/licenses/by/4.0/

e-ISSN: 2148-6905

(Ahmad *et al*., 2020). A review of the literature reveals that ZnO nanoparticles (ZnONPs) are predominantly synthesized using plant-based methods in the green synthesis process (Alavi & Nokhodchi *et al.,* 2021; Bhardwaj *et al.,* 2017; Bhuyan *et al.,* 2015; Brady *et al.,* 2023; Chauhan *et al.,* 2015; Chaurasia *et al.,* 2010; Cooper *et al.,* 1955). However, in the green synthesis approach, various microorganisms, including fungi, bacteria, and algae, can also be utilized alongside plants for the production of ZnO nanoparticles (ZnONPs). Among these, fungi play a particularly significant role by utilizing microbial cells, enzymes, proteins, and other biomolecules to drive the synthesis of ZnO nanoparticles. In this process, ZnONPs can be obtained in the desired size and shape by optimizing the reaction conditions during microbial synthesis**.** The production method used determines the morphology and size of nanoparticles. ZnONPs can exhibit a diverse range of morphologies, including nanoflowers, nanowires, nanorods, nanopellets, nanosprings, nanoplates, nanorings, nanocombs, nanohelix, nanosheets, nanospheres, and nanourchins, which differ in size and shape from other nano-metal oxides (Rajiv *et al.,* 20132). In contrast to expensive and environmentally harmful chemical or physical methods, fungal-mediated synthesis offers cleaner, environmentally friendly, non-toxic, and biocompatible alternative. In the recent years, various fungal species have been used to produce chemical-free and non-toxic ZnO nanoparticles, particularly in biomaterial applications. Fungi can produce metal oxide nanoparticles with minimal energy, thus making them increasingly become prominent in the production of ZnO nanoparticles in recent years. Fungi, offer significant advantages over other microorganisms due to their high metal tolerance, metal absorption capabilities, wide pH-temperature range, rapid accumulation, and cost-effectiveness. ZnONPs synthesized via fungi have stable, biocompatible, and antibacterial properties. ZnONPs exhibit broad-spectrum antibacterial and antifungal activities. They are particularly promising for combating fungal infections, including those caused by multi-drug-resistant fungal strains. These nanoparticles can serve as an alternative approach to deal with the growing threat of drug-resistant fungal infections (Pesika *et al.,* 2003). Therefore, they are widely utilized in various industries including, biomedicine, environmental cleaning, food preservation, agriculture, textile, and pharmaceutical distribution. Especially, the biological applications of nanoparticles are influenced by several factors, as size, shape, surface properties, chemical composition, solubility, and dispersion (Patterson *et al.,* 1939).

Although, in recent years, there have been some studies that explored the production of zinc oxide nanoparticles (ZnONPs) using fungi, these studies remain relatively limited (Dhillon *et al.,* 2012; Venkatesh *et al.,* 2013; Vettumperumal *et al.,* 2016; Wang *et al.,* 2017; Yavuz & Yılmaz, 2021). Abdelhakim *et al.* synthesized ZnONPs using *Alternaria tenuissima* fungus and investigated their light scattering, zeta potentials, antimicrobial, anticancer, antioxidant, and photocatalytic activities (Guilger-Casagrande, M., & de Lima, 2019). Chauhan et al. conducted a study on the synthesis of ZnONPs using *Pichia fermentans* JA2 fungus and their structural, surface, optical, and antibacterial effects (Gupta *et al.,* 2024). Vlad et al. investigated the behaviors of a group of ZnO molecules. In this study, polyurethanes were examined, and a widespread presence of *Aspergillus brasiliensis* was observed. The biological activity was evaluated, and numerous films were created to defend against the attack of Sabouraud-Agar fungi in a nutrient medium. The fungus growth was monitored visually. The study revealed that polyurethane membranes, which have been modified with zinc nanoparticles, possess unique antibacterial and antifungal characteristics, making them essential in medical and biological applications (Günay *et al.,* 2021).

Rajan *et al.* utilized *Aspergillus fumigatus* JCF for the synthesis of zinc oxide (ZnO), resulting in the formation of white agglomerates composed of zinc oxide nanoparticles. The antimicrobial efficacy of these nanoparticles against Gram-positive and Gram-negative bacteria including *Klebsiella pneumoniae*, *Escherichia coli*, and *Pseudomonas aeruginos*a was investigated. The findings of the study demonstrated the efficacy of zinc oxide in effectively combating these harmful microorganisms (Jain *et al.,* 2023). Mohamed et al. synthesized ZnONPs using two recently isolated strains of fungi, *Fusarium keratoplasticum* (A1-3) and

Aspergillus niger (G3-1). Variations in the size, shape, and structure of the biosynthetic ZnONPs were assessed. This study examines the impact of microbial biostimulation using composite ZnONPs and investigates the structural properties of green composite ZnONPs. The properties, antimicrobial activities, and cytotoxic properties of various biosynthesized NPs were analyzed (Jain *et al.*, 2014). Ahmad *et al.* synthesized ZnO from three types of fungi: *D. seriata*, *B. dothidea* and *A. mali*. ZnONPs functioned as inhibitors in addressing fungal diseases in apple orchards. The results suggest that zinc oxide nanoparticles can significantly contribute to combatting fungal pests and improve the protection of plants (Kalpana *et al.*, 2018). Garrett *et al.* produced ceramic ZnO nanoparticles using three different filamentous fungi: *Aspergillus* sp., *Penicillium* sp., and *Paecilomyces variotti*). They used different zinc sources during the production process. Particle sizes ranged from 1 nm to 1000 nm. They synthesized zinc oxide nanoparticles (ZnO) exhibiting conical, cubic, and spherical morphologies (Kalpana *et al.*, 2022). However, there still remain numerous unexplored aspects regarding the green synthesis of ZnONPs using fungi.

In studies of this nature, the antifungal efficacy is influenced by the size and morphology of the antifungal agent. The morphology of ZnO nanoparticles can be regulated by selecting appropriate synthesis methods. The existing literature indicates a substantial number of studies that focused on the production of ZnONPs utilizing plant extracts; however, research involving fungi for ZnONP synthesis remains relatively limited. Various fungal species, including *Psathyrella candolleana*, *Pichia kudriavzevii*, *Aspergillus aereus*, *Fusarium solani*, and *Alternaria alternate*, have been investigated for their potential in the production of zinc oxide nanoparticles (ZnONPs) (Rajiv *et al.*, 2013; Sarkar *et al.*, 2014; Senthilkumar & Sivakumar, 2014; Singh & Singh, 2019; Soosen *et al.*, 2009; Tauc & Menth, 1972; Urbach, 1953; Vlad *et al.*, 2012).

The aim of our study is to determine the effect of fungi on the structural, morphological, elemental, antibacterial and optical properties of ZnO nanoparticles, with particular focus on the role of fungal species and metal precursors in the production of ZnO NPs. ZnO nanoparticles are produced by fungi through the interaction between fungal exudates and metal ions of ZnO. Fungi reduce metal ions to NPs by producing extracellular reducing enzymes that interact with metal ions. Moreover, during this synthesis process, nanoparticles are coated with biomolecules produced by the fungus, increasing the stability and biological activity of the NP (Yoldas & Partlow, 1985; Zeghoud *et al.*, 2022). Metal nanoparticles can be produced from several fungal species such as *Fusarium* sp., *Aspergillus* sp., *Verticillium* sp. and *Penicillium* sp. (Vettumperumal *et al.*, 2016; Wang *et al.*, 2017; Yavuz & Yılmaz, 2017; Yoldas & Partlow, 1985; Zeghoud e*t al.*, 2022). However, the factors that affect this process, such as physical, chemical, and biochemical parameters, remain inadequately understood.

In this study, we used the fungal species Penicillium citrinum, Fusarium solani, Aspergillus flavus and Aspergillus Niger, which have previously been reported to have high reductase activity and high yields in AgNP synthesis. The study also compared the effects of these fungal species on the structural, morphological, elemental, antimicrobial and optical properties of ZnONPs.

2. MATERIAL and METHODS

2.1. Obtaining Fungal Cultures

In this study, the biosynthesis method successfully yielded ZnONPs without the need for hazardous chemical agents. ZnONPs were produced via the biosynthesis method using four different fungal isolates *Penicillium citrinum*, *Fusarium solani*, *Aspergillus flavus*, and *Aspergillus niger*. Each fungal strain was inoculated into 250 ml erlenmeyer flasks containing 160 ml of fungal broth medium and agitated at 25 °C, 125 rpm. Subsequently, the flasks were placed in a water bath for incubation over a period of 7 days. After a 7-day incubation period, the fungal strains were filtered through filter paper and subsequently washed three times with

sterile distilled water to eliminate any residual media components. This process resulted in the collection of the fungal biomass. Each of these fungal masses was placed in 250 ml Erlenmeyer flasks containing 160 ml sterile distilled water. The flasks were then incubated in a shaking water bath at a temperature of 125 rpm for 48 hours. Then, the cell-free filtrates were filtered through filter paper, and the remaining filtrate was used to synthesize ZnONPs. Experimental studies regarding the production of fungal cultures are presented in Figure 1, and the biomass of the fungi used for establishing the fungal cultures can be found in Table 1.

Table 1. Fungal biomass used in obtaining fungal culture.

Fungal Culture	Code	Fungal Biomass (gr)
Penicillium citrinum	*(P.C)*	8.05
Fusarium solani	*(F.S)*	3.70
Aspergillus flavus	*(A.F)*	5.09
Aspergillus niger	*(A.N)*	5.52

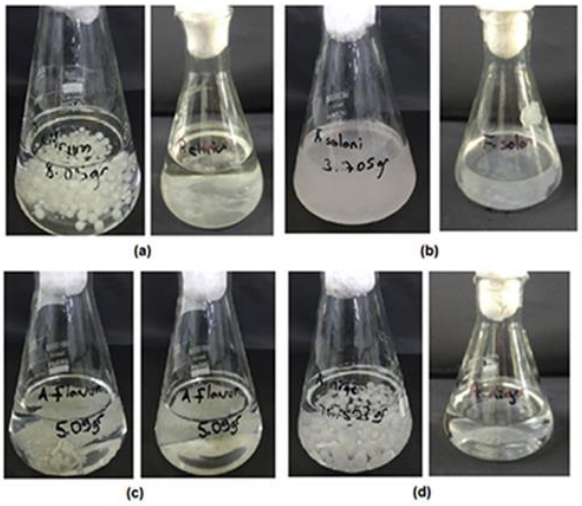

Figure 1. Fungal culture production stages (a) *P. citrinum* (b) *F. solani* (c) *A. flavus* (d) *A. niger*.

2.2. Biosynthesis of ZnONPs Using Cell-Free Filtrate

For four distinct fungal isolates, namely *P. citrinum*, *F. solani*, *A. flavus* and *A. niger*, 2 mM (6.92 g) zinc acetate [$Zn(CH_3CO_2)_2$] was added individually to 160 ml of cell-free filtrate and left for 48 hours at 125 rpm and 25 °C. Subsequently, these solutions were incubated in a water bath with vigorous shaking, yielding four different ZnONPs using cell-free filtrates obtained from the four respective fungal isolates. Figure 2 displays the images of the cell-free filtrates employed as the initial solution for the ZnONPs.

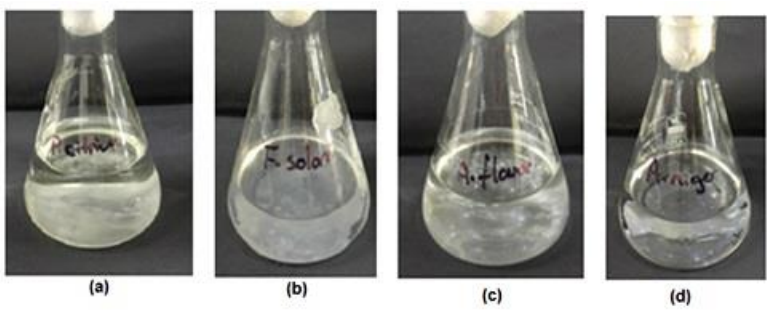

Figure 2. Cell-free filtrates obtained from fungal cultures (a) *P. citrinum* (b) *F. solani* (c) *A. flav*us (d) *A. niger*.

2.3. Obtaining ZnONPs from ZnO Solutions Prepared in Different Fungal Isolates

ZnO nanoparticles (ZnONPs) were synthesized using ZnO solutions derived from different fungal isolates. The solutions of ZnO prepared from the fungal isolates *P. citrinum*, *F. solani*, *A. flavus*, *A. niger* were combined and stirred at 85 °C for 5 hours to gelate the solutions. The method involved heating the gelled ZnO solutions at 400 °C for 10 minutes, yielding slightly yellow- and off-white powder samples of ZnONPs.

2.4. Characterization of ZnONPs

The physical and antibacterial properties of the green synthesized ZnONPs were assessed through range of characterization techniques. The UV-Vis spectra were scanned at wavelengths of 200-800 nm using the SHIMADZU UV-1800 instrument and the data was collected through using UV-Probe software program. The absorbance spectra of ZnONPs were analyzed using the obtained spectra, and the nanoparticles' band gaps, radii, Urbach energies and steepness parameters were determined. The X-ray diffraction (XRD) (Rigaku Ultima-IV) and field emission scanning electron microscopy (FESEM) (Carl Zeiss-Sigma 300 VP) were applied to investigate the structural, morphological and elemental properties of ZnONPs. Additionally, the antibacterial activity of ZnONPs was assessed using the agar diffusion method.

3. RESULTS

3.1. Structural Properties of ZnONPs

Figure 3 illustrates the XRD patterns of ZnONPs generated through green synthesis techniques employing a range of fungal isolates. The patterns were utilized to determine the structural characteristics of the ZnO nanoparticles (ZnONPs), including their phases, Miller indices, grain sizes, and dislocation. As per Figure 3, all films exhibited a hexagonal wurtzite ZnO structure (JCPDS: 04-005-4711), and none of the fungal isolates led to any structural alterations in the nanoparticles. The synthesis of ZnO nanoparticles was successfully achieved using four different selected isolates. The crystallization levels and half-peak widths of all ZnONPs are nearly identical, except for those produced with the *A. flavus* fungal isolate. The crystallization level of ZnONPs produced solely by the *A. flavus* isolate was found to be lower than that of other ZnONPs, and the peak widths were larger. Some structural parameters of ZnONPs, including diffraction angle (2θ), interplanar distance (d), Miller indices (hkl), full width at half maximum (FWHM), grain size (G) and dislocation density (δ) were determined. The grain size and dislocation density of the ZnONPs were calculated using the Scherrer equation (Kumar *et al.*, 2022).

$$D = \frac{0.9\,\lambda}{\beta \cos\theta} \tag{1}$$

$$\delta = \frac{1}{D^2} \tag{2}$$

where λ is wavelength, β is full width at half maximum, θ is Bragg angle and D is grain size. These values are given in Tables 2.

Bragg reflections found in the structures of ZnONPs; produced in *P. citrinum* isolate, correspond to values of 31.7124°, 34.385°, and 36.205°. It was observed that there was dominant growth in the (100), (002), and (101) planes. The grain sizes for these three predominant orientations were calculated, and they were found to be 51.5 nm, 58.1 nm, and 51.6 nm. Additionally, it was observed that the dislocation density in the structured nanoparticles had similar values to the grain size. Bragg reflections can be observed in ZnONPs produced by the *F. solani* isolate at values of 31.725°, 34.384°, and 36.209°, indicating that the (100), (002), and (101) planes exhibited dominant growth. The grain sizes of these three dominant orientations were calculated to be 60.0 nm, 62.4 nm, and 60.6 nm. Bragg reflections were observed in the structures of ZnONPs produced in *A. niger* isolates. The values for these

reflections were 31.705°, 34.336° and 36.2191°. It was noted that there was dominant growth in the (100), (002) and (101) planes. The grain sizes for these three dominant orientations were calculated to be 60.0 nm, 61.6 nm and 61.0 nm, respectively. Bragg reflections in the structures of ZnONPs produced in *A. flavus* isolates correspond to values of 31.782°, 34.417°, and 36.250°. It was observed that dominant growth occurred in the (100), (002), and (101) planes. The grain sizes for these three dominant orientations were calculated to be 45.8 nm, 46.1 nm, and 44.1 nm, respectively.

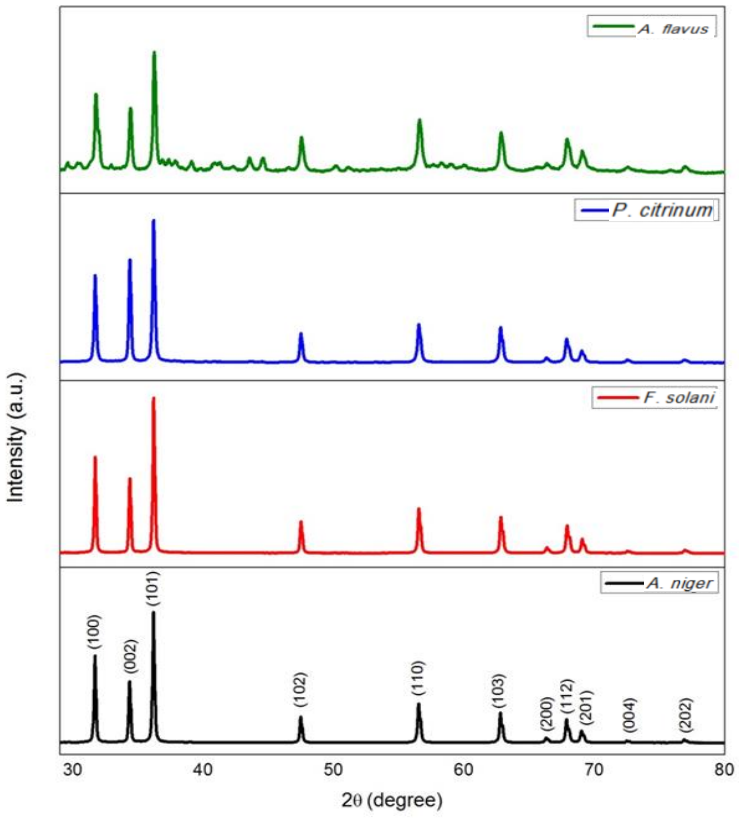

Figure 3. The XRD pattern of ZnONPs.

When examining all films, it was discovered that the grain sizes in the dominant orientations were consistent across each film. Notably, the utilization of the *Aspergillus flavus* isolate in the production of ZnO nanoparticles resulted in the smallest grain size when employing these methods. Furthermore, various unique peaks were identified in these ZnONPs at 10°-25° diffraction angles, which were not present in the other films, indicating possible impurities. Similar structures have also been observed in various studies in the literature on ZnO nanoparticles that were prepared using different methods (Charmaine *et al.*, 2022). The ZnONPs produced by the *P. citrinum* isolate exhibited a dislocation density of 3.77, 2.96, and 3.76 line/nm^2. The (100), (002), and (101) planes experience dominant growth. The dislocation density of zinc oxide nanoparticles (ZnONPs) in *F. solani* isolates was determined to be 2.78, 2.57, and 2.72 line/nm^2 for growth in (100), (002), and (101) planes, respectively. Technical term abbreviations were defined at their first occurrence in the text. Similarly, the dislocation density of ZnONPs produced in *A. niger* isolates was found to be 2.78, 2.64, and 2.69 line/nm^2 for dominant growth in (100), (002), and (101) planes. The dislocation density of zinc oxide nanoparticles (ZnONPs) produced by *A. flavus* isolates corresponds to values of 4.71, 5.14, and 9.13 lines/nm^2. Dominant growth was observed in the (100), (002), and (101) planes. All nanoparticles were found to grow in the smallest grain size (002) orientation. Notably, only the grain size and dislocation density values differ in the ZnONPs produced by the *A. flavus* isolate. It was observed that the stress level in ZnONPs was the highest despite its smallest grain size compared to other nanoparticles.

Table 2. Some of the structural parameters of ZnONPs.

	2θ (°)	d (Å)	Miller indices (hkl)	FWHM (°)	D (nm)	$\delta \times 10^4$ (Line/nm^2)
ZnONPs-*P.citrinum*	31.724	2.818	(100)	0.167	51.5	3.77
	34.385	2.605	(002)	0.149	58.1	2.96
	36.205	2.479	(101)	0.169	51.6	3.76
	47.480	1.913	(102)	0.174	52.1	3.68
	56.512	1.627	(110)	0.198	47.6	4.41
	62.780	1.478	(103)	0.194	50.2	3.97
	66.274	1.409	(200)	0.213	46.6	4.60
	67.851	1.380	(112)	0.218	45.7	4.79
	68.958	1.360	(201)	0.231	43.6	5.26
	72.481	1.302	(004)	0.198	51.9	3.71
	76.844	1.239	(202)	0.276	38.4	6.78
ZnONPs-*F.solani*	31.725	2.818	(100)	0.143	60.0	2.78
	34.384	2.606	(002)	0.139	62.4	2.57
	36.209	2.478	(101)	0.144	60.6	2.72
	47.497	1.912	(102)	0.145	62.4	2.57
	56.543	1.626	(110)	0.159	59.0	2.87
	62.831	1.477	(103)	0.163	59.6	2.82
	66.351	1.407	(200)	0.170	58.3	2.94
	67.925	1.388	(112)	0.178	56.0	3.19
	69.065	1.358	(201)	0.182	55.3	3.27
	72.521	1.302	(004)	0.241	42.8	5.46
	76.954	1.238	(202)	0.252	42.1	5.64
ZnONPs-*A. niger*	31.705	2.819	(100)	0.143	60.0	2.78
	34.336	2.607	(002)	0.140	61.6	2.64
	36.191	2.479	(101)	0.141	61.0	2.69
	47.481	1.913	(102)	0.145	64.1	2.27
	56.526	1.626	(110)	0.156	60.1	2.77
	62.798	1.478	(103)	0.153	63.3	2.50
	66.306	1.408	(200)	0.164	60.5	2.73
	67.882	1.379	(112)	0.169	59.2	2.85
	69.014	1.359	(201)	0.174	57.9	2.98
	72.507	1.302	(004)	0.163	63.1	2.51
	76.889	1.238	(202)	0.182	58.3	2.94
ZnONPs-*A. flavus*	31.782	2.841	(100)	0.189	45.8	4.71
	34.417	2.603	(002)	0.188	46.1	5.14
	36.250	2.476	(101)	0.198	44.1	9.13
	47.508	1.912	(102)	0.274	33.1	8.35
	56.550	1.626	(110)	0.273	34.6	7.42
	62.829	1.477	(103)	0.265	36.7	5.81
	66.367	1.407	(200)	0.240	41.5	7.63
	67.911	1.379	(112)	0.277	36.2	8.81
	69.070	1.358	(201)	0.299	33.7	2.99
	72.500	1.302	(004)	0.560	18.3	1.38
	76.903	1.238	(202)	0.390	26.9	4.71

Additionally, these nanoparticles were found to exhibit the smallest grain size growth (101). The average grain size values of the major orientations of ZnONPs, generated through fungal isolates obtained from *F. solani*, *A. niger*, and *A. flavus*, were established as 53.7 nm, 61 nm, 61.9 nm, and 45.3 nm, respectively. The ZnONPs generated by the *P. citrinum*, *F. niger* isolates, which share similar structural characteristics; the smallest mean grain size belongs to the ZnONPs produced by *P. citrinum*. The mean grain sizes of the ZnONPs generated by the *F.*

solani and *A. niger* isolates are comparable. Nonetheless, the mean grain size of the ZnONPs generated by the *A. Flavus* isolate was the tiniest. The dislocation density values in the dominant orientations of the ZnONPs produced by fungal isolates from *A. flavus* were calculated to be 3.49 lines/nm², 2.69 lines/nm², 2.70 lines/nm², and 6.32 lines/nm², respectively. Among the ZnONPs produced in *P. citrinum*, *F. solani*, and *A. niger* isolates with, similar structural properties, and the ZnONPs produced in *F. solani* and *A. niger* isolates exhibited the lowest average dislocation density values. The average dislocation density values for ZnONPs produced by *F. solani* and *A. niger* isolates were found to be similar. Nevertheless, the ZnONPs produced by the *A. flavus* isolate exhibited the highest average dislocation density.

3.2. Optical Properties of ZnONPs

UV-Vis spectroscopy was utilized to establish the response of ZnONPs to visible light alongside various optical parameters, including band gap, porosity, Urbach energy and refractive index. Absorbance and transmittance spectra for all materials were recorded in the range of 200-900 nm. The absorbance spectra for ZnONPs are exhibited in Figure 4. In general, the absorbance properties for ZnONPs made utilizing different fungal cultures exhibit notable similarities.

In particular, ZnONPs generated in *P. citrinum* and *A. niger* gave rise to analogous absorbance spectra. The band edges of all ZnONPs were observed to be smooth, with a sharp increase at approximately 340 nm. ZnONPs produced in *F. solani* showed an increase in absorbance values in the visible region. Conversely, the absorbance values of other materials in this region were notably low. For all NPs, absorbance values showed a sharp increase upon transmission of wavelengths below approximately 350 nm. At around 300 nm, the absorption values of all nanoparticles reached their peak. It was discovered that ZnONPs that were synthesized using *F. solani* and *A. flavus* had the highest absorption values in this region. The inflection points in the absorbance spectra were initially identified, and are depicted in Figure 5. These peaks, which represent the highest points on the absorbance spectrum may be correlated with surface plasmon resonance (SPR), which is a unique feature of metal nanoparticles (Moormann & Bachand, 2021).

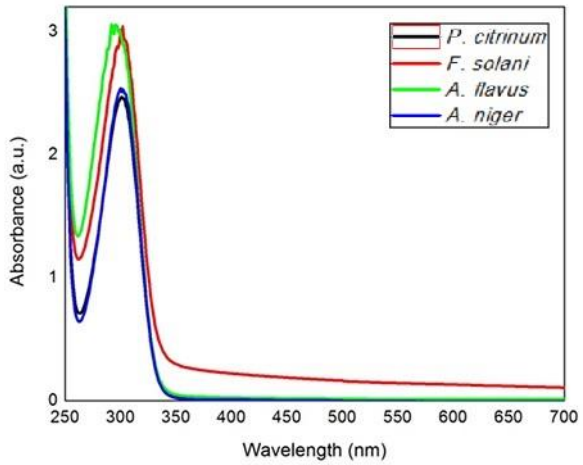

Figure 4. Absorbance spectra of biosynthesized ZnONPs.

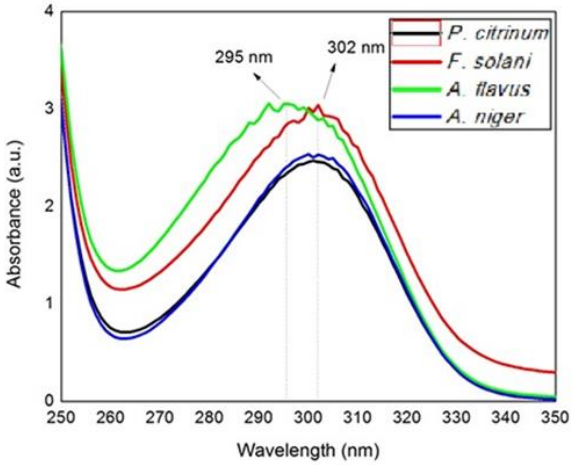

Figure 5. Inflection points in the absorption spectra of ZnONPs.

A shift in the short wavelengths was observed for only one fungal species. This alteration in the absorbance edge may have stemmed from the quantum size effect (Pariona *et al.*, 2020). Particle size was calculated using the effective mass model to characterize the nanoparticle size (r, radius) as it is dependent upon the peak absorbance wavelength (l_p) (Nehru *et al.*, 2023):

$$r\ (nm) = \frac{\left[\frac{1020.72}{\lambda_p} - 26.23012\right]^{1/2} - (0.3049)}{\frac{2483.2}{\lambda_p} - 6.3829} \quad (3)$$

ZnONPs exhibit a peak absorbance of 295 nm and 302 nm, as shown in Figure 8. During the development of equation (3), it was established that m_e = 0.26 m_o, m_h = 0.59 m_o, where m_o represents the free electron mass, ε equals 8.5, and the bulk E_g is 3.3 eV (Mahamuni *et al.*, 2023). Table 3 indicates the sizes of the ZnONPs. A red-shift in the absorbance peak wavelength occurs as the fungal solution varies, attributed to the reduction in quantum confinement resulting from an increase in rising particle size. It was discovered that the absorbance peak of ZnONPs created in the solution of *A. flavus* had shifted to a longer, redder wavelength. Additionally, the particle size was observed to be larger in size. Figure 6 illustrates the transmittance spectra of ZnONPs. The visible region demonstrates high transmittance for all ZnONPs, whereas only those produced in the *F. solani* medium exhibit low transmittance values. This indicates that ZnONPs generated in *F. solani* medium are applicable for absorbing properties, and that those derived in *P. citrinum, A. flavus*, and *A. niger* environments are fit for high transmittance applications.

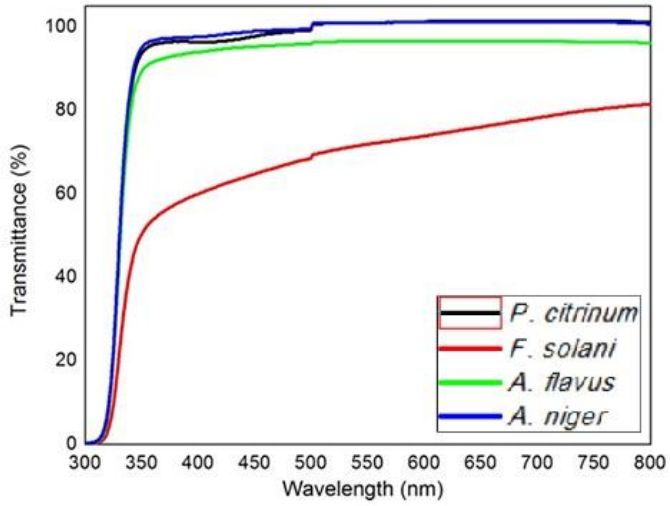

Figure 6. Transmittance spectra of ZnONPs.

Band gap values are crucial optical parameters for technological applications in nanomaterials. Figure 7 presents the αhv^2-hv graphs for ZnONPs and Table 3 displays the band gap (E_g) values derived from these graphs. Based on the results of the analysis of the graphs, it was found that the band gap values of ZnONPs were relatively consistent, measuring at 3.83 eV. The band gap values of ZnO nanoparticles (ZnONPs) produced exclusively in *F. solani* medium are lower than those of other materials. It is evident that the fungal biosynthesis approach has an impact on the band gap values of ZnONPs. The production method yields ZnONPs with enhanced values and a broader band gap. The optical band gap values were calculated using the following equation (Malaikozhundan *et al.*, 2017):

$$(\alpha hv) = A(hv - E_g)^n \quad (4)$$

where A is a constant determined by the refractive index of the material, E_g represents the optical band gap, and hv is the photon energy. The absorption spectra of ZnONPs were used to calculate the average particle size.

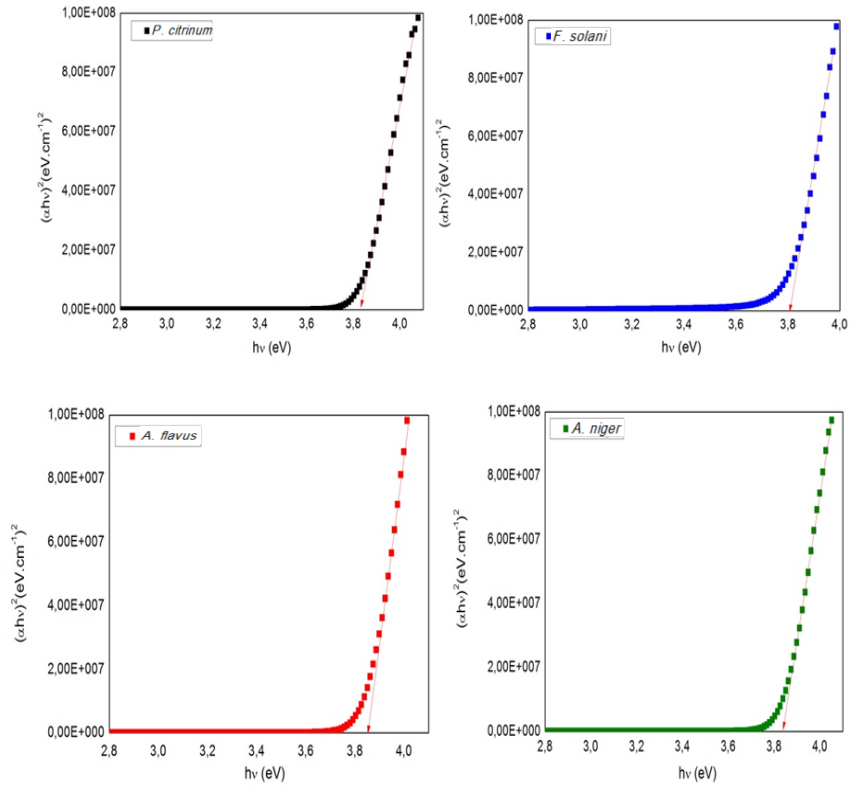

Figure 7. $\alpha h\nu^2$-$h\nu$ graphics of ZnONPs.

Optical transitions between a material's valence and conduction bands, defect states, conduction mechanisms, and disproportionate charge-induced defects depend on the material's bandgap. The identification of these changes and defects in the structure is achieved through detecting the Urbach tails that are formed in the band structure. The energy associated with these Imperfect Urbach tails in the band structure is known as the Urbach energy. Therefore, it is a significant parameter in identifying alterations in the band structure of materials. The Urbach energy was determined by computing the inverse of the gradient of lnα-hν plots, using the following equation (Meruvu *et al.*, 2011):

$$\alpha = \alpha_0 exp^{h\nu - E/E_u} \quad (5)$$

where α_0 is a constant and E_u represents the Urbach energy, which is the width of the tails of localized states in the material's band gap. *lnα-hν* graphs are presented in Figure 8. Another significant parameter that illustrates changes in the band structure is the steepness factor. This parameter is a perpendicularity parameter that indicates the material's band broadening. Additionally, this parameter determines the electron-phonon interaction's potency. Both of these critical parameters can be calculated using the following equations (Moghaddam et al., 2015; Moghaddam *et al.*, 2017):

$$\sigma = \frac{k_B T}{E_u} \quad (6)$$

where σ is the steepness parameter, k_B is the Boltzmann constant, and T is the absolute temperature. The electron-phonon interaction strength ($E_{e\text{-}p}$) depends on the steepness parameter and can be determined using the formula 2/3s. Also, the refractive index of ZnO-NP was calculated through the use of the Ravindra relation (Mohamed *et al.*, 2019). This relationship is linked to the material's band gap of the material, and the equation is provided below:

$$n = 4.084 - 0.62E_g \quad (7)$$

where E_g represents the optical band gap energy calculated from the Tauc plot, and n signifies the refractive index. Furthermore, Figure 9 presents the variations in the optical bandgap-

Urbach energy and optical bandgap values. The porosity values of ZnONPs have been assessed using Equation (8), a quantitative analysis of porosity based on refractive index (Molina *et al.*, 2020):

$$Porosity\ (\%) = \left[1 - \frac{n^2-1}{n_d^2-1}\right] \times 100 \quad (8)$$

where n is the refractive index of ZnONPs and n_d is the refractive index value of pore-free ZnO according to literature. Table 3 presents the calculated values of refractive index and porosity. The results demonstrate that ZnONPs exhibit refractive index values ranging from 1.70 to 1.72 and porosity values of 34.5 % to 35.9 %.

Table 3. The some optical parameters of ZnONPs.

ZnONPs	Peak absorbance peak	Particle R (nm)	E_g (eV)	E_u (meV)	Steepness parameter ($\sigma \times 10^{24}$)	Refractive index (n)	Porosity (%)
P. citrinum	302	1.672	3.83	572	6.58	1.7094	35.9
F. solani	302	1.672	3.81	541	6.96	1.7218	34.5
A. flavus	295	1.581	3.84	566	6.65	1.7032	36.6
A. niger	302	1.672	3.83	571	6.60	1.7094	35.9

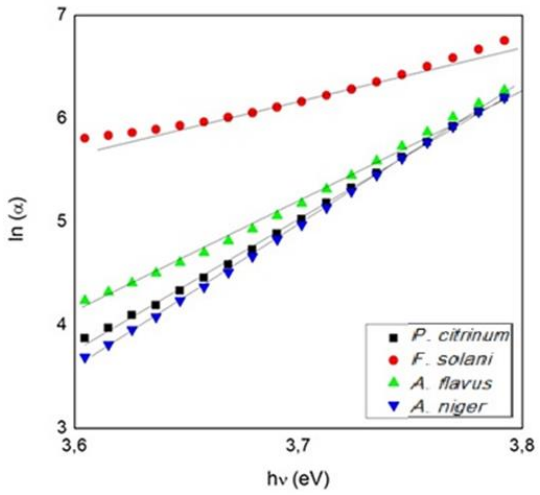

Figure 8. *lnα-hν* graphs of ZnONPs.

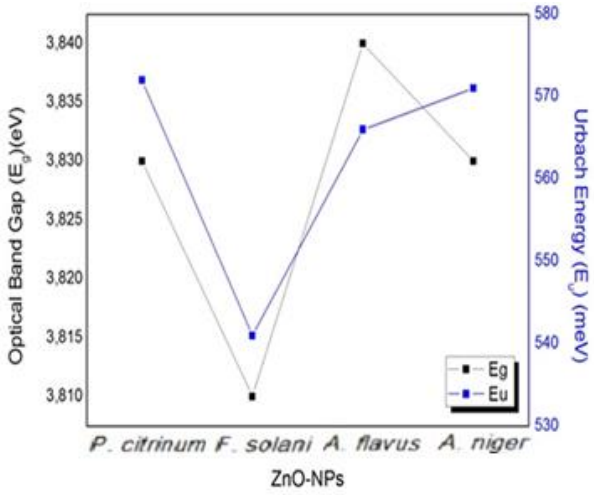

Figure 9. Variation of optical band gap with Urbach energy of ZnONPs.

3.3. Morphological Properties of ZnONPs

Morphological properties of ZnONPs produced in fungal isolates of *P. citrinum*, *A. niger*, *F. solani*, and *A. flavus* were investigated using scanning electron microscopy at 500 x and 3 kx magnifications. FESEM images and the EDX images and elemental analysis findings of ZnONPs are shown in Figure 10 and 11 for *P. citrinum*, *A. niger*, *F. solani*, and *A. flavus* isolates, respectively. When the morphological structures of ZnONPs were examined, it was observed that they all exhibited tightly packed formations, each developing its own distinct morphology. At high magnification (300 kx), the distinct morphologies of all nanoparticles become evident. Nonetheless, upon closer inspection, it was deduced that the morphologies of ZnONPs generated in *P. citrinum* and *A. niger* isolates were corresponding to each other. In Figure 10(a) and 10(c), ZnONPs display a morphology resembling that of cauliflower. Figure 10 reveals that ZnO nanoparticles synthesized by the *P. citrinum* isolate formed larger aggregates, while those produced by the *A. niger* isolate formed smaller clusters. It was observed that both isolates were capable of producing ZnONPs with a cone-shaped morphology.

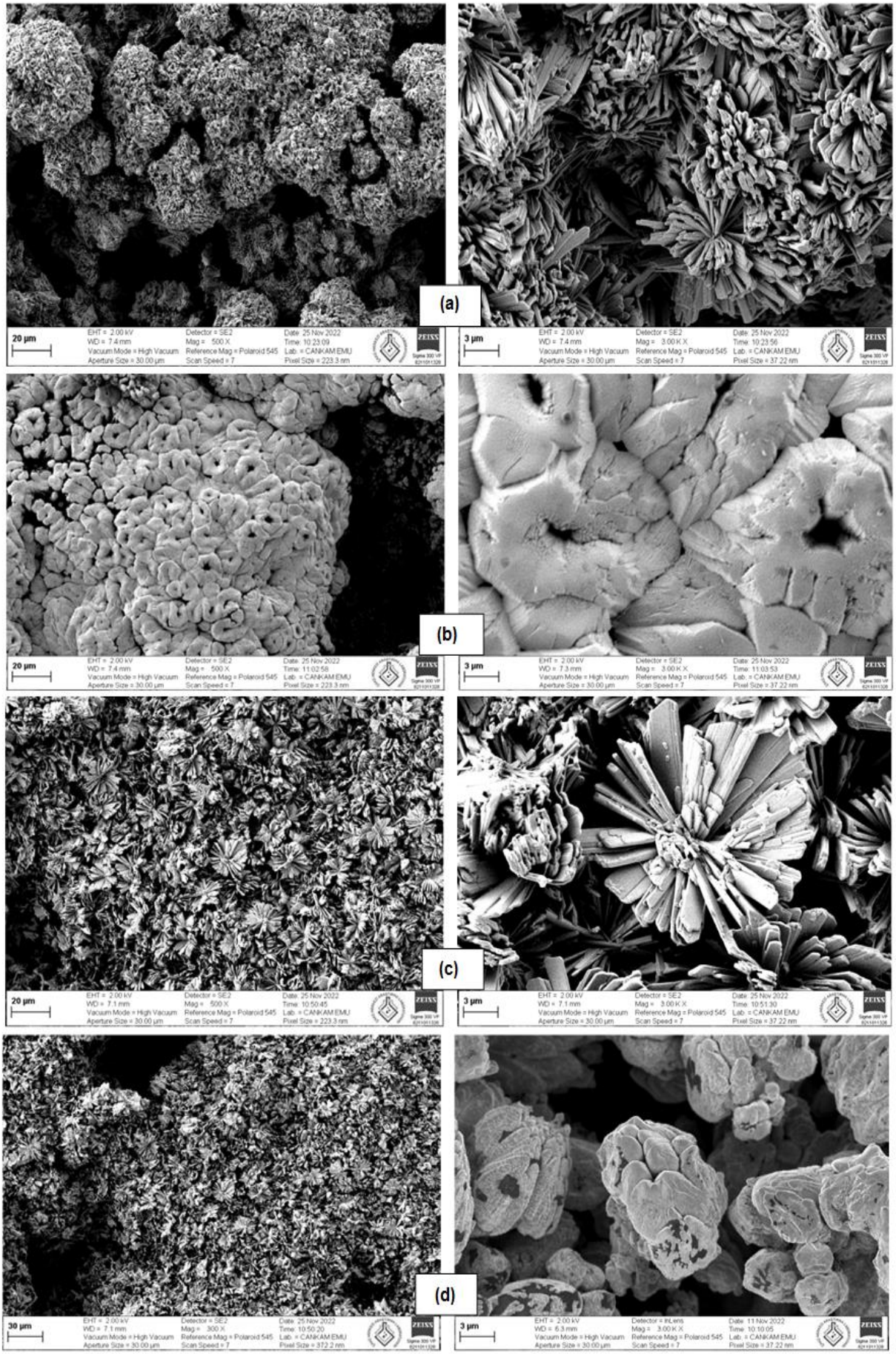

Figure 10. FESEM images of ZnONPs.

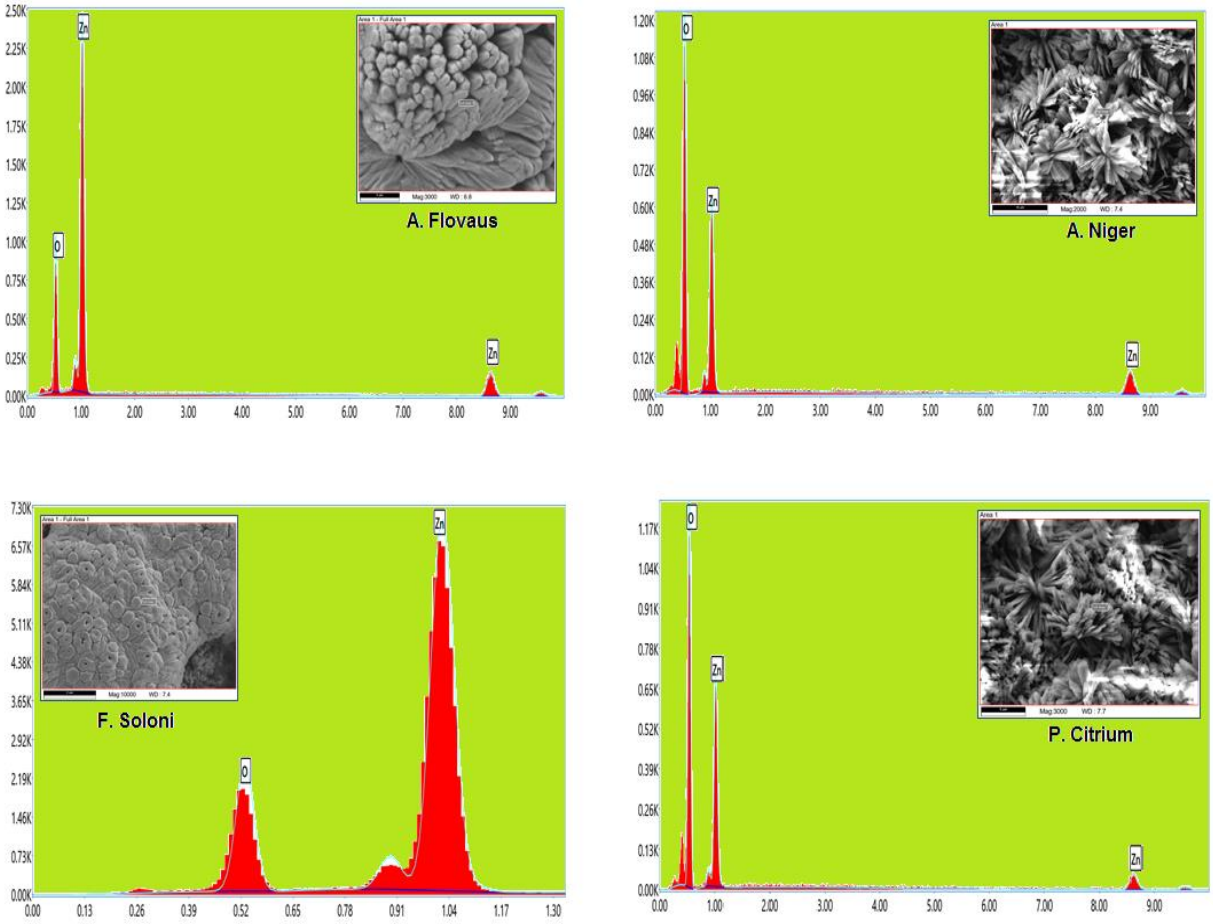

Figure 11. EDX results of ZnONPs.

In addition, the production of nanoparticles in *A. niger* isolation permits for cone-shaped expansion in larger dimensions (Figure 10(c)). Figures 10(b) and 10(d) exhibit the morphologies of ZnONPs created in the *F. solani* and *A. flavus* isolates, respectively. It has been observed that the production of ZnONPs in these isolates resulted in nanoparticles with dissimilar morphologies compared to other isolates. In Figure10(d), ZnONPs created from the *F. solani* isolate displayed greater porosity than nanoparticles produced from other isolates. However, these nanoparticles exhibit a densely packed structure with a void in the center. FESEM images of ZnONPs produced in *A. flavus* isolates are presented in Figure 10(d). It was observed that the ZnONPs had distinct morphologies. A compact, uniform, and foliaceous growth was witnessed for ZnONPs produced in this isolate.

Elemental analysis of ZnONPs synthesized by various fungal isolates was conducted using a field-emission scanning electron microscope (FESEM) device. Figure 11 and Table 4 present the EDX images and elemental analysis findings for ZnONPs obtained from *P. citrinum*, *A. niger*, *F. solani*, and *A. flavus* isolates, respectively. The results indicate the presence of zinc and oxygen atoms in the structure of ZnONPs, which is consistent with the XRD results. When examining the atomic percentages of ZnONPs, it becomes apparent that the nanoparticles with the highest stoichiometric value are those produced in *A. flavus* isolate. Therefore, the ZnONPs produced in these isolates are of lower quality. The atomic percentages of O and Zn atoms in these ZnONPs are very similar. Conversely, the atomic percentages of O and Zn in ZnONPs produced in isolates of *P. citrinum*, *A. niger*, and *F. solani* are significantly different leading to lower stoichiometric values. When examining the atomic ratios in the structure of ZnONPs, it was observed that there was an excess of O and a deficiency of Zn in the nanoparticles produced by *P. citrinum* and *A. niger* isolates. In contrast, the nanoparticles synthesized from the *F. solani* isolate exhibited an excess of zinc and a deficiency of oxygen in their structure. This modified

ratio of Zn and O in the structure is the primary reason for the alteration in the morphology of ZnONPs. The cone-shaped morphological structure of Zn-rich ZnONPs is found to be impaired. This indicates that various fungal isolates are effective in producing ZnONPs with varying atomic percentages.

Table 4. EDX data of ZnONPs.

ZnONPs	Atomic %		Weight %	
	Zn	O	Zn	O
P. citrinum	18.13	81.87	47.51	52.49
F. solani	76.96	23.04	93.17	6.83
A. flavus	40.22	59.78	73.32	26.68
A. niger	23.26	76.74	55.33	44.67

4.4. Antibacterial Properties of ZnONPs

The antibacterial properties of ZnONPs synthesized by various fungal isolates using the biosynthesis method were evaluated through the agar diffusion technique. Using the agar well diffusion method, this study examines the antibacterial impact of ZnONPs on five types of bacteria, namely *Candida albicans*, *Streptococcus mutans* ATCC 10449 s, *Pseudomonas aeruginosa* ATCC 27853, *Eosinophilic pneumonia* NRLLB4420, and *Staphylococcus aureus* ATCC 25923. The minimum inhibitor concentrations were determined by spreading the selected microorganisms onto nutrient agar medium, introducing wells into the medium, and planting sterile vials. The minimum inhibitor concentrations were determined by spreading the selected microorganisms onto nutrient agar medium, introducing wells into the medium, and planting sterile vials. 100 µL of the pertinent biosynthesis product was added to the wells and incubated at 37 °C for 24 hours. Subsequently, the culture dishes were inspected after which the resulting area dimensions were determined. The zone of inhibition (ZOI) was evaluated using the following formula (Moormann & Bachand, 2021):

$$W = \frac{(T-D)}{2} \tag{9}$$

in which *W* represents the width of ZOI (mm), D indicates the diameter of the test specimen (mm), and T refers to the total diameter of the said specimen. These computed figures and the zone of inhibition are illustrated in Table 5 and Figure 13, correspondingly.

Figure 12(a) presents the examination of the antimicrobial properties of biosynthesized ZnO-NP on various fungal isolates, including *P. citrinum*, *F. solani*, *A. flavus* and *A. niger*. It was found that ZnONPs exhibited a significant antibacterial effect against *Candida albicans* microorganisms. Moreover, their resistance to specified microorganism was observed. Notably, the antibacterial effect varied among different fungal isolates against *Candida albicans* microorganisms. The ZOI widths of ZnONPs for this microorganism ranged from 4.2 to 4.5 cm. The *A. flavus* fungal isolate produced ZnONPs with the highest antibacterial activity against the *Candida albicans* microorganism. The smaller particle size of this particular ZnONPs, along with its surface morphology, supports its superior antibacterial activity compared to other ZnONPs. This is because the small size and protruding surface morphology of the particles enable them to penetrate into the cell more effectively, thereby increasing antibacterial resistance (Qianwei *et al.*, 2022; Rajan *et al.*, 2016). Figure 12(b) demonstrates the evaluation of antimicrobial activity of biosynthesized ZnONPs against *Eosinophilic pneumonia* microorganisms using fungal isolates of *P. citrinum*, *F. solani*, *A. flavus* and *A. niger*. The findings suggest that ZnO-NP had limited antibacterial effects against Eosinophilic pneumonia microorganisms and their high resistance against this substance was clear. While the ZnONPs synthesized from the *F. solani* and *A. flavus* isolates exhibited different antibacterial effects on the microorganisms responsible *for Eosinophilic pneumonia*, the other ZnONPs showed consistent antibacterial effects. The ZOI widths of the ZnONPs, which were produced these

isolates against, this microorganism varied from 0.5 to 0.7 cm. *F. Solani* fungal isolate displayed the most potent antibacterial activity towards microorganisms that cause eosinophilic pneumonia. Figure 12(c) displays the evaluation of the antimicrobial impact of biosynthesized ZnONPs on Pseudomonas aeruginosa microorganisms through fungal isolates of *P. citrinum*, *F. solani*, *A. flavus* and *A. niger*. It was found that ZnONPs demonstrated limited antibacterial efficacy against *Pseudomonas aeruginosa* microorganisms with ZOI widths of 0.5 to 0.6 cm.

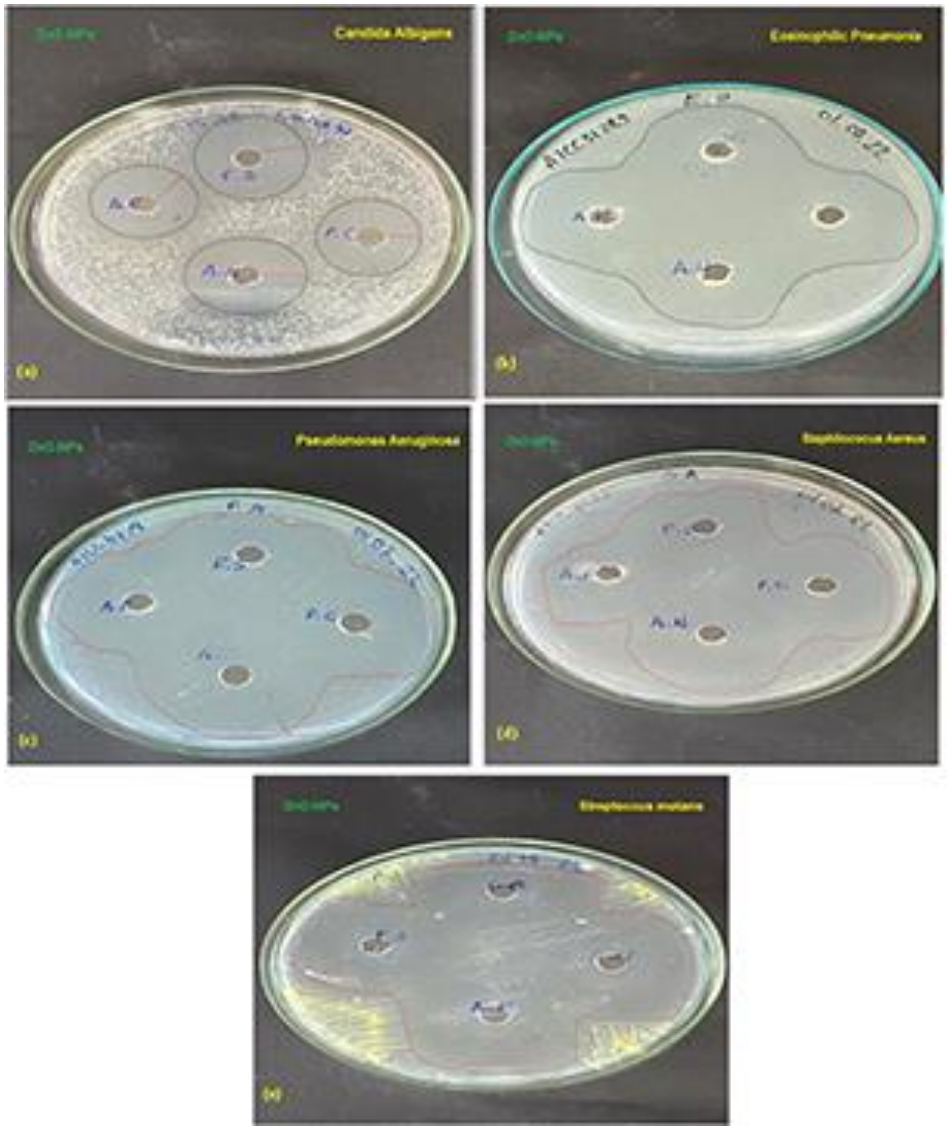

Figure 12. Antibacterial activity tests of ZnONPs (a) *Candida albicans* (b) *Eosinophilic pneumonia* (c) *Pseudomonas aeruginosa* (d) *Staphylococcus aureus* and (e) *Streptococcus mutans* microorganisms.

It was observed that the antibacterial effect of various fungal isolates on the microorganism *Pseudomonas aeruginosa* remained consistently similar. While ZnONPs produced by the *F. solani* fungal isolate exhibited differing antibacterial activity on *Pseudomonas aeruginosa* microorganisms, the remaining three isolates demonstrated identical antibacterial effects. Figure 12(d) displays the results of the testing undertaken to determine the antimicrobial effect of ZnONPs synthesized biologically on the microorganism *Staphylococcus aureus* through the utilization of fungal isolates such as *P. citrinum*, *F. solani*, *A. flavus*, and *A. niger*. Analysis revealed that ZnONPs provided a weaker antibacterial effect on the microorganism *Staphylococcus aureus* compared to other variations of ZnONPs. The ZOI widths of ZnONPs for this microorganism ranged from 0.1 to 0.9 cm. It was noted that the antibacterial impact of various fungal isolates on *Staphylococcus aureus* microorganisms was equal. However, the *A. niger* fungal isolate demonstrated the highest antibacterial activity on *Staphylococcus aureus* microorganisms, as it produced ZnONPs. Figure 12(e) displays the assessment of the

antibacterial properties of biosynthesized ZnO-NPs on *Streptococcus mutans* microorganisms using fungal isolates of *P. citrinum*, *F. solani*, *A. flavus*, and *A. niger*. It was found that ZnONPs exhibited a significant antibacterial effect on Streptococcus mutans. The ZOI widths of ZnONPs for this microorganism ranged from 2.1 to 2.4 cm. It was observed that the antibacterial effect of various fungal isolates on the microorganism *Streptococcus mutans* was comparable. The ZnONPs produced in both *P. citrinum* and *F. solani* fungal isolates exhibited uniform antibacterial activity on *Streptococcus mutans* microorganisms, with *A. flavus* isolates presenting with the slowest antibacterial activity.

As a result of the antimicrobial effectiveness test, it became apparent that the biosynthetic products harvested from the fungal mass had an antimicrobial effect on all the microorganisms tested. Figure 13 displays the variation in the inhibition zone of ZnONPs created from various fungal isolates on different bacteria. Similarly, Figure 14 illustrates the juxtaposition of the inhibition diameters of ZnONPs on the identical bacteria. All ZnONPs exhibited significant antibacterial activity against *Candida albicans* and *Streptococcus mutans*. However, while all ZnONPs had low antibacterial activity against Staphylococcus bacteria, those produced in the *A. niger* isolate demonstrated high resistance. The antibacterial effects of ZnONPs were similar in other bacterial species.

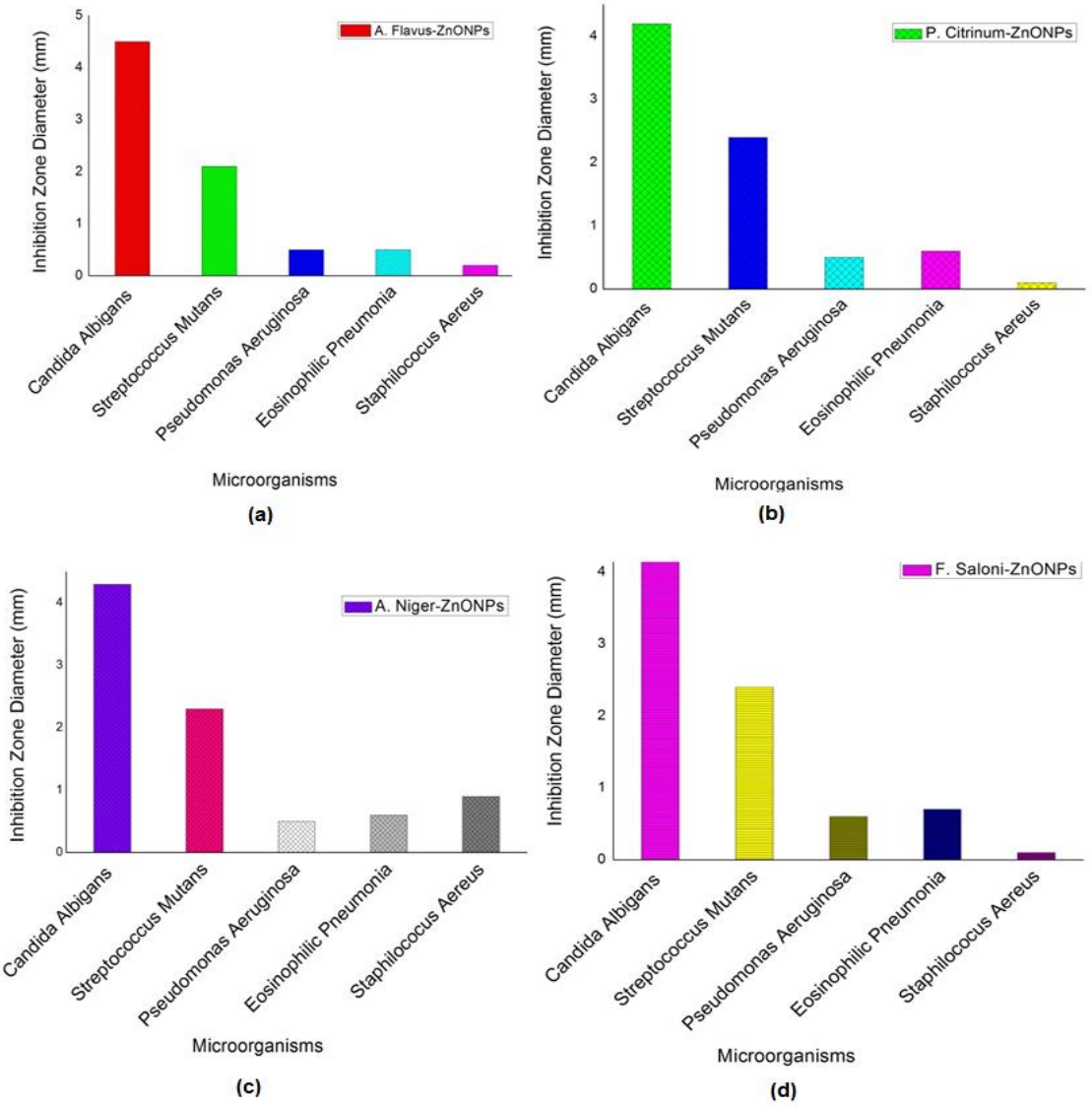

Figure 13. The inhibition zone variation of ZnONPs (a) *A. flavus*, (b) *P. citrinum*, (c*) A. niger* and (d) *F. solani.*

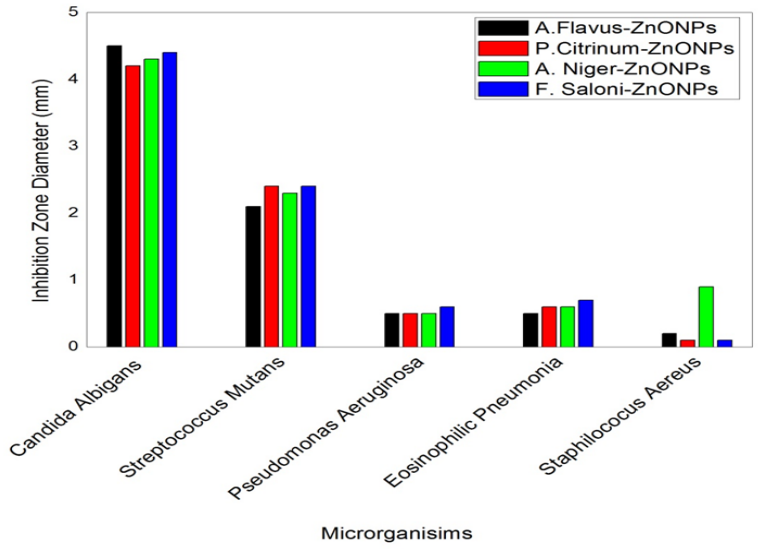

Figure 14. The comparison of the inhibition diameters of ZnONPs on the same bacteria.

Table 5. The zone of inhibition (ZOI) values of ZnONPs.

Bacteria	ZnONPs			
	P. citrinum	*F. solani*	*A. flavus*	*A. niger*
Candida albicans	4.2 cm	4.4 cm	4.5 cm	4.3 cm
Streptococcus mutans ATCC 10449 s	2.4 cm	2.4 cm	2.1 cm	2.3 cm
Pseudomonas aeruginosa ATCC 27853	0.5 cm	0.6 cm	0.5 cm	0.5 cm
Eosinophilic pneumonia NRLLB4420	0.6 cm	0.7 cm	0.5 cm	0.6 cm
Staphylococcus aureus ATCC 25923	0.1 cm	0.1 cm	0.2 cm	0.9 mm

4. DISCUSSION and CONCLUSION

In this study, zinc oxide nanoparticles (ZnONPs) were produced successfully using various fungal cultures. The chosen fungal species for ZnONPs production were observed to have substantial impacts on the physical and antibacterial characteristics of the nanoparticles. As a result of the structural analysis of the nanoparticles, it was found that all fungal cultures were appropriate for the production of ZnONPs. The ZnONPs, formed under hexagonal zinc oxide structure and dominant orientations, were identical in all cases. However, in ZnONPs produced solely in *A. flavus* mushroom culture, different phases formed within the structure, and the crystallization level was lower. The average grain size of the ZnONPs is between 53-61 nm. It was determined that ZnONPs synthesized through *P. citrinum* culture had the smallest grain size and the most favorable structure. ZnONPs synthesized from *P. citrinum*, *A. flavus*, and *A. niger* cultures were highly transparent (at a rate of 90%). The least transparent ZnONPs were synthesized from *F. solani* culture nanoparticles. Particle radii and bandgap values were measured to be in the range of 1-2 nm at 3.83 eV. It was determined that the bandgap, refractive index, and porosity values of the fungal cultures used did not affect the particle size but did affect other aspects of the nanoparticles. ZnONPs displayed high levels of resistance against *Candida albicans* and *Streptococcus mutans* bacteria. Furthermore, in contrast to other types of nanoparticles, ZnONPs produced from the *A. niger* fungal culture exhibited greater resistance against *Staphylococcus aureus* bacteria. Furthermore, the fungal diversity induced significant alterations in the morphological architecture of ZnONPs. The nanoparticles synthesized from *P. citrinum* and *A. niger* fungal cultures resembled each other with their nano-flake structure, while ZnONPs generated from *A. flavus* and *F. solani* fungal cultures adopted distinct morphological compositions.

Consequently, ZnONPs produced with different fungi can be utilized as an alternative biomaterial in applications such as an alternative filling and bracket material, particularly in dental applications due to their in vitro antimicrobial properties against *Candida albicans* and *Streptococcus mutans* bacteria.

Acknowledgments

This study is produced from the Master thesis "Production and Characterization of ZnO Nanoparticles by Biosynthesis" prepared by Mohanad Fawzi Mutar Mutar in 2023 under the supervision of Assoc. Prof. Dr. Olcay Gençyılmaz. We would also like to thank Prof. Dr. Rasime Demirel from Eskişehir Technical University for her help in providing fungi cultures.

Declaration of Conflicting Interests and Ethics

The authors declare no conflict of interest. This research study complies with research and publishing ethics. The scientific and legal responsibility for manuscripts published in IJSM belongs to the authors.

Authorship Contribution Statement

Olcay Gençyılmaz: Conceptualization, Methodology, Validation, Data curation, Writing – review & editing, Writing – original draft, Supervision. **Mohanad Fawzi Mutar Mutar:** Methodology and Writing – original draft.

Orcid

Olcay Gençyılmaz https://orcid.org/0000-0002-7410-2937
Mohanad Fawzi Mutar Mutar https://orcid.org/0009-0008-1285-8342

REFERENCES

Abdelhakim, H.K., El-Sayed, E.R., & Rashidi, F.B. (2020). Biosynthesis of zinc oxide nanoparticles withantimicrobial, anticancer, antioxidant and photocatalytic activities by theendophytic *Alternaria tenuissima*. *Journal of Applied Microbiology*, *128*, 1634–1646. https://doi.org/10.1111/jam.14581

Ahmad, H., Venugopal, K., Rajagopal, K., De Britto, S., Nandini, B., Pushpalatha, H.G., & Jogaiah, S. (2020). Green synthesis and characterization of zinc oxide nanoparticles using Eucalyptus globules and their fungicidal ability against pathogenic fungi of apple orchards. *Biomolecules*, *10*(3), 425. https://doi.org/10.3390/biom10030425

Alavi, M., & Nokhodchi, A. (2021). Synthesis and modification of bio-derived antibacterial Ag and ZnO nanoparticles by plants, fungi, and bacteria. *Drug Discovery Today*, *26*(8), 1953-1962. https://doi.org/10.1016/j.drudis.2021.03.030

Bhardwaj, N., Gaur, A., & Yadav, K. (2017). Effect of doping on optical properties in $BiMn_{1-x}(TE)_xO_3$ (where x= 0.0, 0.1 and TE= Cr, Fe, Co, Zn) nanoparticles synthesized by microwave and sol-gel methods. *Applied Physics A*, *123*(6), 429-436. https://doi.org/10.1007/s00339-017-1042-y

Bhuyan, T., Mishra, K., Khanuja, M., Prasad, R., & Varma, A. (2015). Biosynthesis of zinc oxide nanoparticles from *Azadirachta indica* for antibacterial and photocatalytic applications. *Materials Science in Semiconductor Processing*, *32*, 55-61. https://doi.org/10.1016/j.mssp.2014.12.053

Brady, N.G., O'Leary, S.L., Moormann, G.C., Singh, M. K., Watt, J., & Bachand, G.D. (2023). Mycosynthesis of Zinc Oxide Nanoparticles Exhibits Fungal Species Dependent Morphological Preference. *Nano-Micro Small, 19(15),* 2205799. https://doi.org/10.1002/smll.202205799

Chauhan, R., Reddy, A., & Abraham, J., (2015). Biosynthesis of silver and zinc oxide nanoparticles using Pichia fermentans JA2 and their antimicrobial property. *Applied Nanoscience*, *5*, 63–71. https://doi.org/10.1007/s13204-014-0292-7

Chaurasia, V., Chand N., & Bajpai, S.K. (2010). Water Sorption Properties and Antimicrobial Action of Zinc Oxide Nanoparticles-Loaded Cellulose Acetate Films. *Journal of*

Macromolecular Sciencer Part A: Pure and Applied Chemistry, *47*, 1-9. https://doi.org/10.1080/10601320903539207

Cooper, K.E. (1955). Theory of Antibiotic Inhibition Zones in Agar Media. *Nature 176*, 510–511. https://doi.org/10.1038/176510b0

Dhillon, G.S., Brar, S.K., Kaur, S., & Verma, M. (2012). Green approach for nanoparticle biosynthesis by fungi. *Critical Reviews in Biotechnology*, *32(1)*, 49-73. https://doi.org/10.3109/07388551.2010.550568

Guilger-Casagrande, M., & de Lima, R. (2019). Synthesis of Silver Nanoparticles Mediated by Fungi: A Review. *Frontiers in Bioengineering and Biotechnology*, *7*(287), 1-16. https://doi.org/10.3389/fbioe.2019.00287

Gupta, S., Ravi, R.K., & Pathak, B. (2024). Photocatalytic Removal of Anthracene Using Zinc Oxide Nanoparticles Synthesized by Fusarium proliferatumWC416. *Geomicrobiology Journal*, *41*(1), 72-81, 10. https://doi.org/1080/01490451.2023.2272621

Günay, K., Leblebici, Z., & Koca, F.D. (2021). Biosynthesis, characterization and anti-bacterial effect of zinc nanoparticles (ZnO NP). *Nevşehir Journal of Science and Technology*, *10*(1), 56-66. https://doi.org/10.17100/nevbiltek.917256

Jain, N., Bhargava, A., Tarafdar, J.C., Singh, S.K., & Panwar, J. (2013). A biomimetic approach towards synthesis of zinc oxide nanoparticles. *Applied Microbiology Biotechnology*, *97*, 859–869. https://doi.org/10.1007/s00253-012-3934-2

Jain, N., Bhargava, A., & Panwar, J., (2014). Enhanced photocatalytic degradation of methylene blue using biologically synthesized “protein-capped” ZnO nanoparticles. *Chemical Engineering Science*, *243*, 549–555. https://doi.org/10.1016/j.cej.2013.11.085

Kalpana, V.N., Kataru, B.A.S., Sravani, N., Vigneshwari, T., Panneerselvam. A., & Rajeswari, V.D. (2018) Biosynthesis of zinc oxide nanoparticles using culture filtrates of *Aspergillus niger:* Antimicrobial textiles and dye degradation studies. *Opennano*, *3*, 48-55. https://doi.org/10.1016/j.onano.2018.06.001

Kalpana, V.N., Kataru, B.A.S., Sravani, N., Vigneshwari, T., Panneerselvam, A., & Rajeswari, V.D. (2022). *Annona reticulata* leaves-assisted synthesis of zinc oxide nanoparticles and assessment of cytotoxicity and photocatalytic impact. *Materials Letters*, *309*, 131379. https://doi.org/10.1016/j.matlet.2021.131379

Kumar, R.V., Vinoth, S., Baskar, V., Arun, M., & Gurusaravanan, P. (2022). Synthesis of zinc oxide nanoparticles mediated by *Dictyota dichotoma* endophytic fungi and its photocatalytic degradation of fast green dye and antibacterial applications. *South African Journal of Botany*, *15*, 337-344. https://doi.org/10.1016/j.sajb.2022.03.016

L. Nehru, G. D. Kandasamy, V. Sekar, M. Ali Alshehri, C. Panneerselvam, A. Alasmari, & P. Kathirvel, (2023). Green synthesis of ZnO-NPs using endophytic fungal extract of *Xylaria arbuscula* from *Blumea axillaris* and its biological applications. *Artificial Cells, Nanomedicine, and Biotechnology*, *51*(1), 318-333. https://doi.org/10.1080/21691401.2023.2232654

Mahamuni Badiger, P., Ghare, V., Nikam, C., & Patil, N. (2023). The fungal infections and their inhibition by Zinc oxide nanoparticles: an alternative approach to encounter drug resistance. Nucleus, 1-19. https://doi.org/10.1007/s13237-023-00439-1

Malaikozhundan, B., Vaseeharan, B., Vijayakumar, S., Pandiselvi, K., Kalanjiam, M.A.R., Murugan, K., & Benelli, G. (2017). Biological therapeutics of *Pongamia pinnata* coated zinc oxide nanoparticles against clinically important pathogenic bacteria, fungi and MCF-7 breast cancer cells. *Microbial Pathogenesis*, *104*, 268-277. https://doi.org/10.1016/j.micpath.2017.01.029

Meruvu, H., Vangalapati, M., Chippada, S.C., & Bammidi, S.R. (2011). Synthesis and characterization of zinc oxide nanoparticles and its antimicrobial activity against *Bacillus subtilis* and *Escherichia coli. Rasayan Journal of Chemistry*, *4*(1), 217–222.

Moghaddam, A.B, Namvar, F., Moniri, M., Tahir, P.M., Azizi, S., & Mohamad, R. (2015). Nanoparticles Biosynthesized by Fungi and Yeast: A Review of Their Preparation,

Properties, and Medical Applications. *Molecules*, *20*, 16540-16565. https://doi.org/10.3390/molecules200916540

Moghaddam, A.B., Moniri, M., Azizi, S., Rahim, R.A., Ariff, A.B., Saad, W.Z., Namvar, F., Navaderi, M., & Mohamad, R. (2017). Biosynthesis of ZnO Nanoparticles by a New *Pichia kudriavzevii* Yeast Strain and Evaluation of Their Antimicrobial and Antioxidant Activities. *Molecules*, *22*, 872. https://doi.org/10.3390/molecules22060872

Mohamed, A.A., Fouda, A., Abdel-Rahman, M.A., Hassan, S.D., El-Gamal, Salem, M.S., & Shaheen, S.S. & (2019). Fungal strain impacts the shape, bioactivity and multifunctional properties of green synthesized zinc oxide nanoparticles, *Biocatalysis and Agricultural Biotechnology*, *19*, 101103. https://doi.org/10.1016/j.bcab.2019.101103

Molina, D.A., Giner-Casares, J.J., & Cano, M. (2020). Bioconjugated Plasmonic Nanoparticles for Enhanced Skin Penetration. *Topics in Current Chemistry*, *378(8)*, 1-17. https://doi.org/10.1007/s41061-019-0273-0

Moormann, G.C., & Bachand, G.D. (2021). Biosynthesis of Zinc Oxide Nanoparticles using Fungal Filtrates. *Sand 2021*, 9437R.

Moormann, G.C., & Bachand, G.D. (2021). Biosynthesis of Zinc Oxide Nanoparticles using Fungal Filtrates. *Center for Intergarted Nanotechnologies* (CINT), 9437R, 1-4. https://doi.org/10.2172/1817833

Pariona, N., Paraguay-Delgado, F., Basurto-Cereceda, S., Morales Mendoza, J.E., Hermida-Montero, L.A., & Mtz-Enriquez, A.I. (2020). Shap dependent antifungal activity of ZnO particles against phytopatogenic Fungi. *Applied Nanoscience*, *10*, 435–43.

Patterson, A.L. (1939). The Scherrer Formula for X-Ray Particle Size Determination. *Physical Review Journals*, *56*, 978. https://doi.org/10.1103/PhysRev.56.978

Pesika, N.S., Stebe, K.J., & Searson, P.C. (2003). Relationship between absorbance spectra and particle size distributions for quantum-sized nanocrystals. *The Journal of Physical Chemistry B, 107(38)*, 10412–10415. https://doi.org/10.1021/jp0303218

Qianwei, L.I., Feixue, L.I.U., Min, L.I., Chen, C., & Gadd, G.M. (2022). Nanoparticle and nanomineral production by fungi. *Fungal Biology Reviews*, *41*, 31e44. https://doi.org/10.1016/j.fbr.2021.07.003

Rajan, A., Cherian, E., & Baskar, G. (2016). Biosynthesis of zinc oxide nanoparticles using Aspergillus fumigatus JCF and its antibacterial activity. *International Journal of Modern Science and Technology*, *1*(2), 52-57.

Rajiv, P., Rajeshwari, S., & Venckatesh, R. (2013). Bio-Fabrication of zinc oxide nanoparticles using leaf extract of *Parthenium hysterophorus* L. and its size-dependent antifungal activity against plant fungal pathogens. *Spectrochimica Acta Part A: Molecular and Biomolecular Spectroscopy*, *112*, 384–387

Sarkar, J., Ghosh, M., Mukherjee, A., Chattopadhyay, D., & Acharya, K. (2014). Biosynthesis and safety evaluation of ZnO nanoparticles. *Bioprocess and Biosystems Engineering*, *37*, 165–171. https://doi.org/10.1007/s00449-013-0982-7

Senthilkumar, S.R., & Sivakumar T. (2014). Green tea (*Camellia sinensis*) mediated synthesis of zinc oxide (ZnO) nanoparticles and studies on their antimicrobial activities. *Int. J. Pharm. Pharm. Sci.*, *6*(6), 461–465.

Singh, I., & Singh, S., (2019). Study of algal mediated biosynthesis of nanoparticle: future of green nanotechnology. *Current Life Sciences*, *5*(1), 7-14. https://doi.org/10.5281/zenodo.2666643

Soosen, S.M., Bose, L., & George, K.C. (2009). Optical properties of ZnO nanoparticles. *Academic Review*, *16*(1-2), 57–65.

Tauc, J., & Menth, A. (1972). States in the gap. *Journal of Non-Crystal Solids*, *569*, 8–10. https://doi.org/10.1016/0022-3093(72)90194-9

Urbach, F. (1953). The long-wavelength edge of photographic sensitivity and of the electronic absorption of solids. *Physical Review*, *92*(5), 1324. https://doi.org/10.1103/PhysRev.92.1324

Vlad, S., Tanase, C., Macocinschi, D., Ciobanu, C., Balaes, T., Filip, D., & Gradinaru, L.M. (2012). Antifungal behaviour of polyurethane membranes with zinc oxide nanoparticles. *Journal of Nanomaterial Biostructructure*, *7*, 51–58.

Venkatesh, K.S., Palani, N.S., Krishnamoorthi, S.R., Thirumal, V., & Ilangovan, R. (2013). Fungus mediated biosynthesis and characterization of zinc oxide nanorods. *AIP Conference Proceeding*, 1536, 93–94. https://doi.org/10.1063/1.4810116

Vettumperumal, R., Kalyanaraman, S., Santoshkumar, B., & Thangavel, R. (2016). Estimation of electron–phonon coupling and Urbach energy in group-I elements doped ZnO nanoparticles and thin films by sol–gel method. *Materials Research Bulletin*, *77*, 101–110. https://doi.org/10.1016/j.materresbull.2016.01.015

Wang, L., Hu, C., & Shao, L., (2017). The antimicrobial activity of nanoparticles: present situation and prospects for the future. *International Journal of Nanomedicine*, *12*, 1227–49. https://doi.org/10.2147/IJN.S121956

Yavuz, İ., & Yılmaz, E.Ş. (2021), Nanoparticles with Biological Systems, *Journal of Gazi University Science Faculty*, *1*, 93-108. https://doi.org/10.5281/zenodo.4843592

Yoldas, B.E., & Partlow, D.P. (1985). Formation of broad band antireflective coatings on fused silica for high power laser applications. *Thin Solid Films*, *129*(1–2), 1–14. https://doi.org/10.1016/0040-6090(85)90089-6

Zeghoud, S., Hemmami, H., Seghir, B.B., Amor, I.B., Kouadri, I., Rebiai, A., Simal-Gandara, J. (2022). A review on biogenic green synthesis of ZnO nanoparticles by plant biomass and their applications. *Materials Today Communications*, *33*, 104747. https://doi.org/10.1016/j.mtcomm.2022.104747